



# Experimental study on rebound and recompression deformation characteristics of different soils

Jiaqi Dong<sup>1</sup> · Boxin Wang<sup>1</sup> · Qing Wang<sup>1</sup> · Xinchuan Xu<sup>2</sup> · Lina Yang<sup>3</sup>

Received: 24 January 2022 / Accepted: 6 April 2023 / Published online: 25 April 2023  
© Springer-Verlag GmbH Germany, part of Springer Nature 2023

## Abstract

For deep and large foundations, the soil below the foundation is often in a compensated or overcompensated state after the structure is completed. At this time, the proportion of recompression settlement to the total settlement is more significant. Attention should be paid to calculating the rebound deformation and recompression deformation of foundation pit excavation. In this work, the silty clay, clay, and silt in the Binhai New Area of Tianjin were studied. Oedometer tests were carried out on original and remolded samples to investigate the compressibility of different soil samples under unloading/reloading (the minimum unloading pressure ( $P_{\min}$ ) was set to 50, 100, 200, and 400 kPa, and the maximum preloading pressure ( $P_{\max}$ ) was kept at 400, 800, 1200, and 1600 kPa, respectively). The results indicate that the difference between the compressibility of the original and remolded samples decreases with repeated loading. It is also observed that the smaller the  $P_{\min}$  value, the smaller the corresponding difference. Compared with the remolded sample, the original sample has a higher maximum rebound rate ( $\delta_{\max}$ ) and lower recompression rate ( $\lambda$ ). When  $P_{\min}$  is constant, the original and remolded samples show that  $\delta_{\max}$  increases while  $\lambda$  decreases with the increase of  $P_{\max}$ , eventually becoming the same. Clay is the least sensitive to  $\delta_{\max}$  and the most sensitive to  $\lambda$ . Combined with the analysis of pore distribution characteristics, the results indicate that the medium pores converge to the small pores during compression. The conclusion of this study can provide a theoretical basis and support for the design of underground space in coastal areas as well as for deep and large foundation buildings according to deformation control design.

**Keywords** Structural strength · Rebound and recompression · Rebound rate · Recompression rate · Microscopic pores

## Introduction

Certain factors in geotechnical engineering cause soft soils to undergo unloading/reloading cycles, such as preloading, foundation pit excavation, and staged construction. Soft soils undergoing consolidation can lead to major disasters around the world.

Tianjin is located at the confluence of the five major tributaries of the Haihe River in the North China Plain. It

faces the Bohai Sea in the east and Yanshan Mountain in the north. The Haihe River winds through the city. Binhai New Area is in the eastern coastal area of Tianjin, the center of the Bohai Sea Economic Circle. With the development and large-scale construction, making full use of land resources and exploiting underground space have become the primary consideration of the foundation. Excavation unloading and gravity stress release are bound to cause the foundation pit-bottom-soil to rebound, resulting in uplift deformation. From the development trend, the foundation of a high-rise building requires a deep direction of development. With more and more ultra-deep and super-large foundation pit engineering applications, the problems of unloading, rebound, deformation, and recompression of foundation pit excavation are becoming more and more prominent (Teng et al. 2012). Therefore, in-depth understanding and analysis of the compression characteristics of cohesive soils under unloading and reloading during foundation pit engineering will help engineers more accurately predict the settlement

✉ Qing Wang  
wangqing@jlu.edu.cn

<sup>1</sup> College of Construction Engineering, Jilin University, Changchun 130026, People's Republic of China

<sup>2</sup> China Water Northeastern Investigation, Design and Research Co, Ltd, Changchun 130000, People's Republic of China

<sup>3</sup> Jilin University of Architecture and Technology, Changchun 130114, People's Republic of China

and rebound of the soil and design appropriate methods to reduce engineering disasters (Farzad and Hamid 2018; Lyu et al. 2020). Thus, it is necessary to study the rebound and recompression characteristics of the soil layer during loading and unloading.

At present, most of the research is based on remolded soil unloading/reloading. Most modern soil mechanics from reconstituted clays or the results of the study of the characteristics of artificial soil, however, are different from the original clay. Original soils exhibit some form of “structure”. It is usually acknowledged that the structure is formed during their depositional history (Leroueil and Vaughan 1990), signifying the unique arrangement and bonding of the soil constituents that differ from the corresponding reconstructed soils. There are extensive experimental data to suggest that soil structure and stress history are influences of first importance on the mechanical behavior of natural soil (Rowe 1972; Skempton 1985; Burland 1990). The original and remolded samples should be studied separately for analysis and comparison because of the structural existence.

It is well-known that the soil compression curves show unloading/reloading loops. The soil viscosity effect has commonly explained these loops; clayey soils have larger loops because of their relatively higher viscosity, and sandy soils have narrow loops because of their low viscosity, silty soils being between the two. Thus, it can be said that the mechanical properties of soils are mainly affected by the physical properties and particle size composition of the soil. Simultaneously, soil properties are related to the current stress state and depend on the past and recent stress history, that is, the stress path. The stress path method proposed by Lambe (1967) provides a reasonable method for field and laboratory study of soil properties. Silty clay was the research focus of the study. The strength change law under the unloading state was obtained, and the scope of the unloading affected area and the strength attenuation law in the affected area were estimated (Pan et al. 2001). By analyzing the deformation characteristics under unloading action, it was concluded that there is a critical unloading ratio in the rebound deformation of silt, and the rebound deformation is divided into three parts, i.e., primary rebound deformation, secondary rebound deformation, and additional secondary consolidation deformation (Shi et al. 2004). Further, the experimental study on clay was carried out to study the indicators of unloading ratio, rebound rate, and elastic modulus, and the calculation method of unloading rebound amount was proposed (Pan and Hu 2002). It was proposed that the rebound deformation has a critical unloading ratio, and its magnitude is negatively correlated with the preload (Zhang et al. 2008). The analysis of the unloading and reloading processes of natural hard clay under compression can be regarded as a competition between mechanical and physicochemical effects (Cui et al. 2013). The rebound and recompression behaviors of

different types of soils were studied through the stress path (Li et al. 2011), rebound recompression and model tests (Li and Teng 2011), rebound recompression test and actual engineering (Teng et al. 2013a, b), and load test (Li and Teng 2018). Thus, the rebound and recompression deformation was predicted and verified. However, most existing research focuses on the rebound and recompression deformation under complete unloading, i.e., the endpoint of unloading is 0. However, under the influence of various factors, most of the actual projects are incomplete unloading. Thus, it is meaningful to design multiple sets of loading and unloading paths for different soils for analysis.

It has become a common understanding that soil engineering properties depend significantly on microstructure and related structural changes. Soil structure will be damaged and adjusted during compression and rebound, which must be analyzed through micro-scale investigations. The macroscopic properties of soil, such as the mechanical and hydraulic properties, are controlled by its microstructure (Dalla Santa et al. 2019; Delage et al. 2006; Jiang et al. 2014; Zhang et al. 2018, 2020; Wang et al. 2020). Therefore, studying soil pore changes after unloading and reloading from a microscopic perspective can fundamentally analyze the mechanism of soil deformation caused by loading and unloading.

Based on the compressive deformation characteristics of the soils in Tianjin Binhai, this paper analyzes and investigates the structural characteristics of the soil. Meanwhile, multiple sets of unloading, rebound, and compression consolidation tests are set to further analyze the soil rebound and recompression rates during loading and unloading. The mechanical and structural characteristics of soils in Tianjin Binhai New Area were studied by compression and rebound tests and analyzed by combining the microstructural and macro-mechanical characteristics.

## Materials and methods

### Study area and sample properties

The materials studied are cores sampled from Tianjin Binhai New Area, China (Fig. 1a, b) at three depths, namely silty clay (SC) from 7.3 to 7.6 m depth, clay (C) from 14.8 to 15.1 m depth, and silt (S) from 18.8 to 19.1 m depth, as shown in Fig. 1c and d. The basic properties of the tested soil were obtained following the test procedure in GB/T50123 (2019) by parallel testing. Particle size distribution was determined by densimeter and sieve method (Table 1). The result shows that C and SC have a relatively high clay content than S. Figure 2a shows the mineral composition and the mineral contents of the soil determined by X-ray diffraction (XRD). The dominant clay mineral (shown in Fig. 2b) is

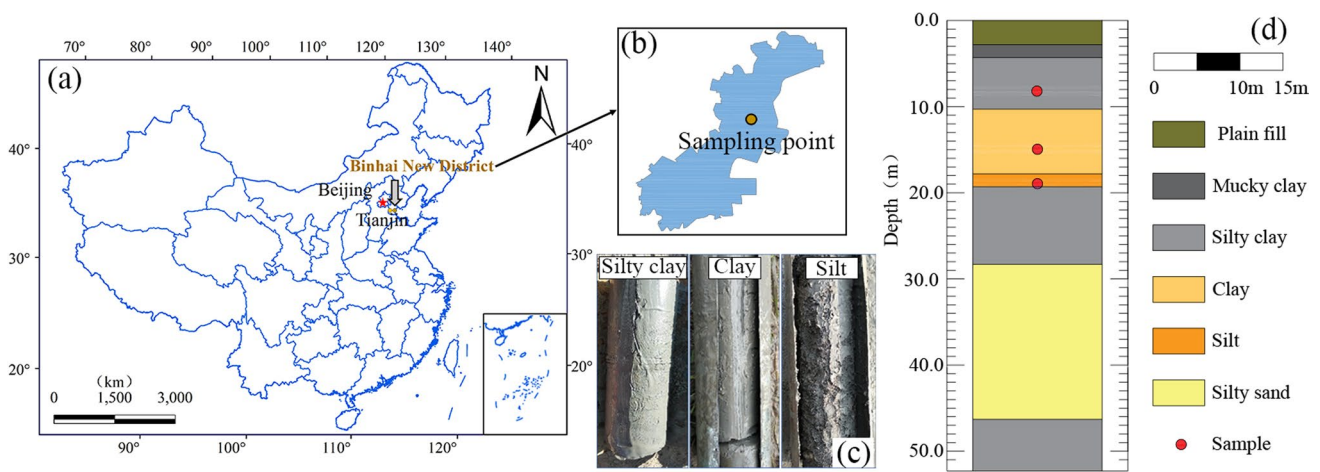


**Fig. 1** Overview of the sampling points: **a**, **b** Geographical position of the study area, **c** field sampling, **d** borehole histogram

**Table 1** Particle size distribution of natural soft soil

Sample	Content of different fraction (%)		
	2~0.075 mm	0.075~0.005 mm	<0.005 mm
SC	5.8	69.57	24.63
C	2.01	71.5	26.49
S	2.49	85.98	11.53

illite, with a relatively small particle size, large specific surface area, and strong water absorption. As shown in Fig. 2c, the organic matter and soluble salt contents showed as follows: C > SC > S, consistent with the clay content distribution. The physical properties are shown in Table 2. Different parameters, such as the specific gravity of solid particles ( $\rho_s$ ), natural moisture content ( $w$ ), void ratio ( $e$ ), liquid limit

( $w_L$ ), plastic limit ( $w_p$ ), and plasticity index ( $I_p$ ), have been reported.

### Test procedures and program

#### Test equipment and sample preparation

In this test, a stress-controlled high-pressure consolidation instrument (Nanjing Soil Instrument Factory) (Fig. 3a) was adopted. The soil samples were drained on both sides. Wet cotton was used to surround the pressurized cover plate during the test to reduce the influence of the surrounding environment on the moisture content of the soil sample. At the same time, the indoor temperature and humidity were adjusted according to the changes in the indoor environment. After the incremental loading procedure, one-dimensional

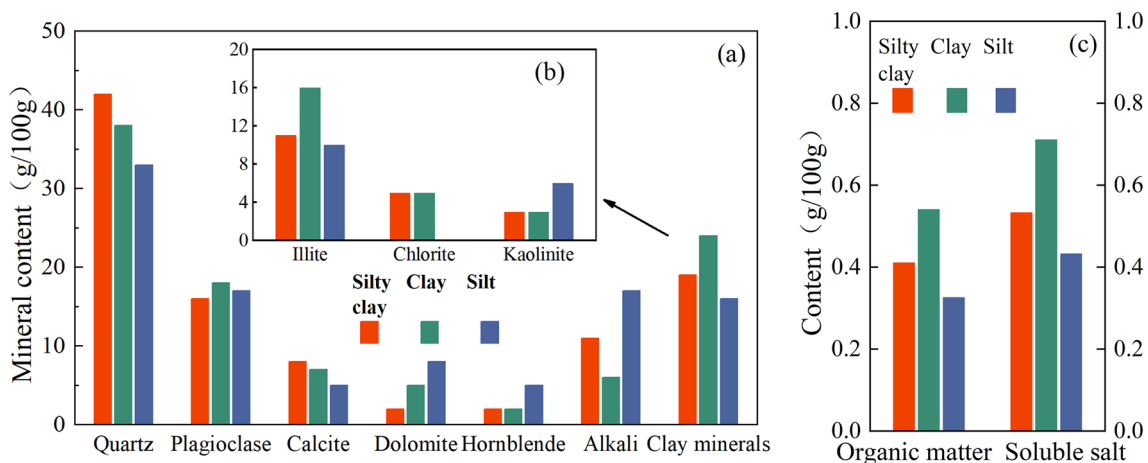


**Fig. 2** Composition of soils: **a** the typical mineral composition of various types of soil, **b** the typical secondary composition of various types of soil, **c** the content of organic matter and soluble salt of various types of soil

**Table 2** Physical characteristic parameters of test soil

Sample	Depth (m)	$\rho_s$ (g/cm <sup>3</sup> )	w (%)	e (-)	w <sub>L</sub> (%)	w <sub>p</sub> (%)	I <sub>p</sub> (-)
SC	7.3–7.6	2.70	28.9	0.76	31.2	18.4	12.8
C	14.8–15.1	2.73	40.2	1.03	47.3	24.7	22.6
S	18.8–19.1	2.69	20.1	0.55	23.8	16.7	7.1

consolidation tests were performed on samples (GB/T50123—2019). Each incremental load was applied for 1 h to eliminate the non-negligible effect of loading periods on the development of soil resistance. The unloading process adopts the same method. Following a 1-h loading period, The oedometer tests were considered feasible on tested samples as the consolidation degree reached more than 90% (Wang and Abriak 2015; Wang et al. 2016). The initial and final loads on the soil sample were set as 12.5 kPa and 1600 kPa, respectively.

Preparation of original soil samples: the original soil samples (300 mm in height, 100 mm in diameter) obtained in the field were sealed, wrapped with plastic wrap, and stored to avoid exposure to sun and rain. Try to prevent water loss in the soil, fix the soil sample and spread air bubble film, sponge, etc., during transportation to avoid the vibration of

the soil sample to keep the soil sample in its original state to the greatest extent. Press the ring knife, whose inner wall is evenly coated with lubricant, into the soil, and then use the soil cutter to trim the two ends of the ring knife. The two ends of the ring knife are trimmed and flattened, and the standard ring knife sample required for the test is prepared (Fig. 3b).

Preparation of remolded soil test: the original soil samples taken at the site were fully air-dried and then crushed. To ensure the structural comparison with the original samples, the moisture content and dry density of the remolded samples were strictly controlled to be consistent with the on-site sampling. The conventional compaction test was used for preparation, and the configured reshaped sample was pressed into a compactor equipped with a ring knife. The required density was achieved through compaction.

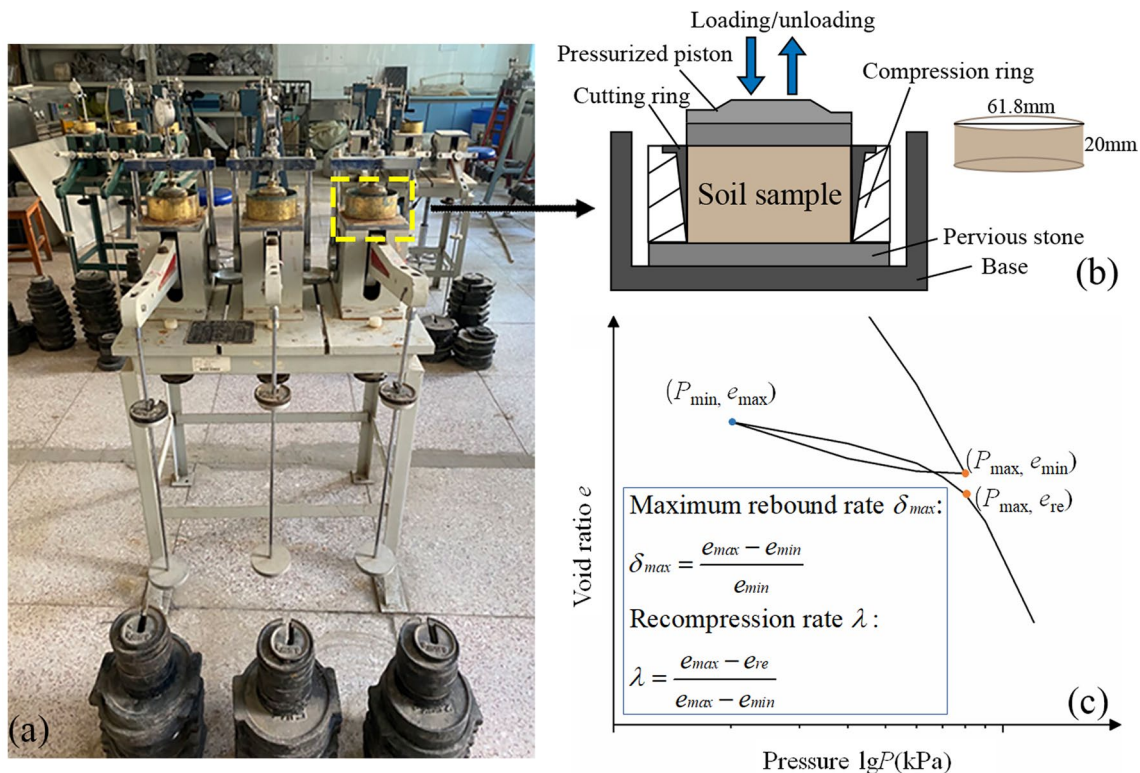


**Fig. 3** Schematic diagram of compression rebound test: **a** a stress-controlled high-pressure consolidation instrument (Nanjing Soil Instrument Factory), **b** loading and unloading operation position detail diagram, **c** schematic diagram of compression rebound



Vaseline was applied to the inner wall of the ring knife to reduce the effect of friction on the compression test.

### Test protocol design

The compressibility index of soil is not constant; it changes with the change in pressure. To study the unloading–reloading characteristics of the original sample and the remolded sample under different minimum unloading pressure, the compression index pressure range under the national standard (GB/T50123-2019) was used for experimental design. Soil compressibility is often defined by the compressibility factor  $a_v$  (when  $a_v < 0.1 \text{ MPa}^{-1}$ , it is low compressibility soil; when  $0.1 \leq a_v < 0.5 \text{ MPa}^{-1}$ , it is medium compressibility soil; when  $a_v \geq 0.5 \text{ MPa}^{-1}$ , it is high compressibility soil). The compression coefficient  $a_v$  used to determine compressibility is chosen for the pressure interval from  $P_1 = 100 \text{ kPa}$  to  $P_2 = 200 \text{ kPa}$  (National Standard GB/ T50123-2019). Therefore, 100 kPa and 200 kPa were selected as the minimum unloading pressures  $P_{\min}$  to analyze the rebound characteristics at different stages. The pressure ratio of the consolidation instrument test is usually set to 1, and the pressures on both sides of the 100–200 kPa stage are selected as 50 kPa and 400 kPa ( $P_{\min}$ ). Thus,  $P_{\min}$  is selected as 50 kPa, 100 kPa, 200 kPa, and 400 kPa. The depth of groundwater level drop in most urban areas of North China (the drop depth is about 50 m) can be regarded as an increase in soil stress of about 400 kPa (Di Prisco et al. 2000; Zhang et al. 2010). The pressure ratio of the consolidation instrument test is usually set to 1. Combined with  $P_{\min}$  (50 kPa, 100 kPa, 200 kPa, and 400 kPa) and other comprehensive considerations, the maximum loading pressure  $P_{\max}$  is selected as 400 kPa, 800 kPa, 1200 kPa and 1600 kPa.

Table 3 presents the vertical consolidation stress and the related cycle of loading/reloading for each sample. According to Table 3, the loading and unloading tests of the original sample and the remodeled sample were carried out. Three parallel tests were carried out for each test plan, and the average value was taken as the test result. In order to reduce human error, the sample preparation process and the test process are all completed by one person. The compression rebound process affects the stability of foundation pit excavation and the effectiveness of groundwater recharge. This time, the maximum rebound rate and reload rate (Teng et al. 2012) (Fig. 3c) are analyzed through the loading–unloading test. The specific parameters are given in Fig. 3c.

To observe the pore distribution and pore characteristics after different loading–unloading intervals, mercury porosimetry tests were carried out on all. The microstructural characteristics the original and the remolded samples were analyzed.

**Table 3** Summary of the tests

Sample type	Test no	$P_{\min}$ (kPa)	$P_{\max}$ (kPa)
Original soil	SC/C/S-400	400	800,1200,1600
	SC/C/S-200	200	800,1200,1600
	SC/C/S-100	100	400,800,1200,1600
	SC/C/S-50	50	400,800,1200,1600
	SC/C/S	Standard consolidation (no unloading)	
Remolded soil	SC/C/S-Re-400	400	800,1200,1600
	SC/C/S-Re-200	200	800,1200,1600
	SC/C/S-Re-100	100	400,800,1200,1600
	SC/C/S-Re-50	50	400,800,1200,1600
	SC/C/S-Re	Standard consolidation (no unloading)	

SC silty clay, C clay, S silt,  $P_{\min}$ : the minimum unloading pressure,  $P_{\max}$  the maximum preloading pressure

## Results and discussion

### Compression characteristics

#### Compression curve analysis

As shown in Fig. 4a, the compression curve ( $e$ - $\lg P$ ) of original soil samples can be divided into three sections: the gentle section, the steep decline section, and the section tending towards the remolded soil compression curve (Shen 1998).

In the initial compression stage, when the pressure is less than the yield pressure of the structure, the compression curve is gentle, and the compression deformation is small. The results indicate that the soil structure remains unchanged under the action of external load. However, only a certain amount of elastic deformation and plastic deformations are generated (the elastic deformation is mainly predominant and has slight structural disturbance, and the pore change of soil is relatively small).

The second stage: the steep decline section, when the pressure is slightly greater than the yield of the stress structure, and the slip between particles is accompanied by the collapse of the structure. Therefore, the proportion of plastic deformation in the overall deformation of the soil will increase significantly.

In the third stage, the deformation increases continuously with the further increase of vertical pressure. Intergranular slip is the primary cause of deformation, indicating that the compression curve of the original sample tends to be consistent with that of the remolded sample. The compression curve of the remolded samples is a straight line because the remolded soil has lost the influence of soil structure.

Figure 4b indicates a certain difference in the compression coefficient between the original soil and the remolded soil (of the same soil kind). The overall performance is that

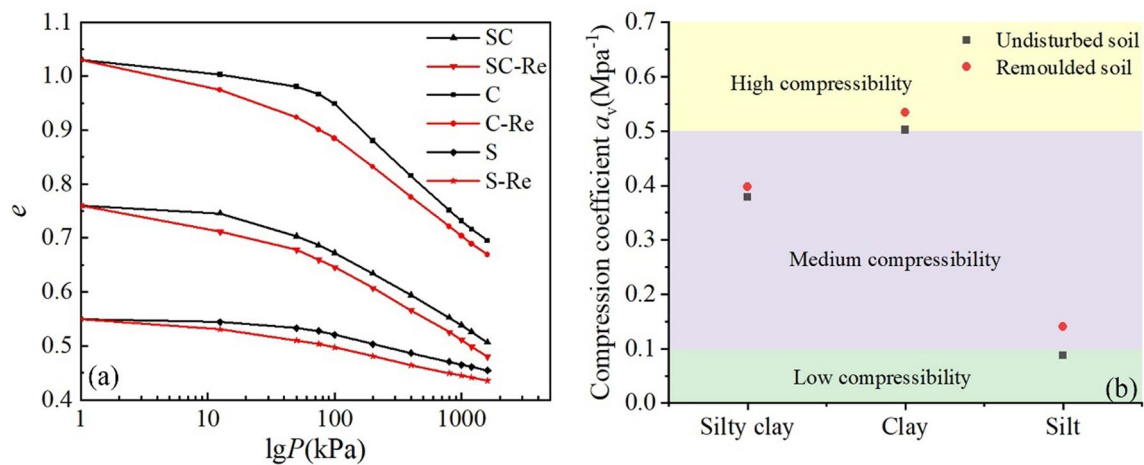


**Fig. 4** Normal standard consolidation: **a** standard compression curve, **b** compression coefficient

the compression coefficient of the remolded soil is greater than that of the original sample. In other words, the compression resistance is less than that of the original soil.

The consistency of other physical and chemical factors was controlled as much as possible during the experiment. According to the analysis, the difference is the structural characteristics of the original soil itself, which affects the mechanical properties of the soil. For the original soil, before the force reaches the initial bonding strength, it is mainly the self-adjustment process of the initial structure, and the deformation is minimal, which shows the linear stress–strain relationship. When most of the damage to the original soil structure has been incurred, and it has lost structural strength due to the application of force, the tiny incremental force will cause deformation of the more significant growth. As the force beyond the structural strength of soil continues to grow, the progression of the deformation and destruction of soil structure occurs. Gradually the new stable secondary structure is formed. The strength of the secondary structure formation due to the progression of external load stress increases the final destruction of the soil at a prolonged rate (Xie and Qi 1999).

#### Determination of pre-consolidation pressure and structural yield stress

For structured soils, the pre-consolidation pressure ( $P_c$ ) is different from that of unstructured soils. Traditionally, the stress measured by the Casagrande method considering the structural characteristics is called the structural yield stress  $\sigma_k$  (Li 1982; Shen 1998). Here, the research method of Xiao Shufang and others (Wang et al. 2005) has been adopted. Using the absence of structural remodeling samples as the basis of the theoretical study, the resultant pressure  $P_c$  of naturally deposited structural soils was determined by reducing

the compression curves of the remodeling samples, and the mathematical model of the reduced compression curves of the remodeling soils was established as follows (Wang et al. 2003, 2005):

$$e = e_1 - C_r(\log P_L)^{1-A} \cdot (\log P)^A, \quad (1)$$

$$\text{Type : } A = 1 + \frac{\log(C_s/C_r)}{\log(\log \sigma_k / \log P_L)}, \quad (2)$$

$e$  represents the void ratio in the reduction compression curve;  $e_1$  represents the void ratio when the pressure is 1 kPa (Commonly initial void ratio  $e_0$  is used instead);  $C_s$  represents the rebound index of the remolded sample;  $C_r$  represents the compression index of the remolded sample;  $\sigma_k$  represents the structural yield stress of the original specimen;  $P_L$  represents the stress value corresponding to the intersection of the compression curve of the remolded sample and the original sample;  $A$  represents the reduction coefficient, which characterizes the compression curve after reduction

The structural yield stress  $\sigma_k$  (Fig. 5a) is determined based on the original test compression curve. Meanwhile, the method of reducing and reshaping the test compression curve is applied to determine the pre-consolidation pressure ( $P_c$ ) of the sample (Fig. 5b). The structural strength  $q$  is the difference between  $P_c$  and  $\sigma_k$ . The structural indicators of the three samples in the study area are shown in Fig. 5b. For structured soils,  $\sigma_k$  is greater than the previous consolidation pressure, which is due to the presence of structure.  $q$  is the difference between the two. The maximum  $q$  value of C is 20 kPa, the minimum of SC is 13 kPa, and the minimum of S is 5 kPa. The structure of the soil is due to the connection of the water film between the particles to connect the adjacent soil together to form a certain cohesive force, the magnitude of which primarily depends on the thickness

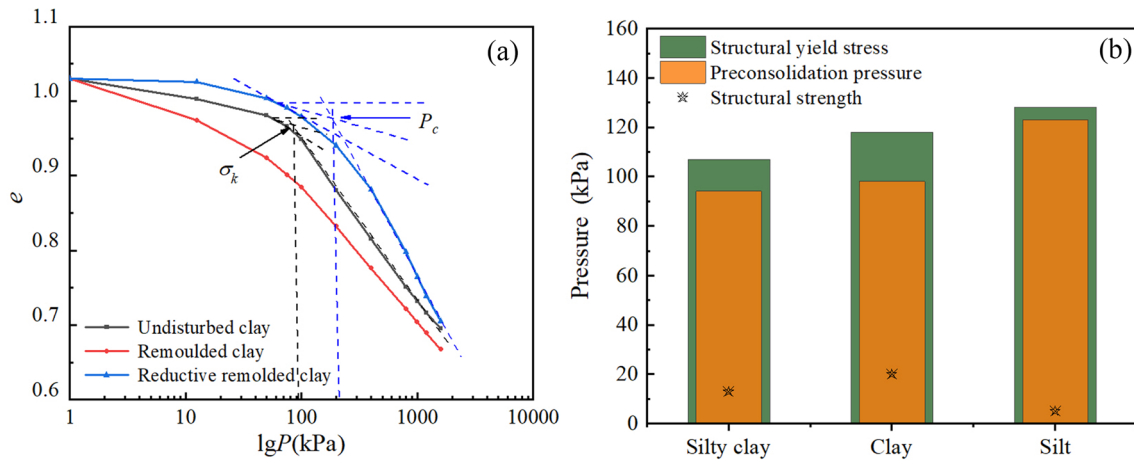


**Fig. 5** Schematic diagram for structural strength acquisition: **a** obtaining the yield stress  $\sigma_k$  and pre-consolidation pressure of the structure  $P_c$ , **b** structural strength  $q$

of the combined water film. The structural strength results show that the structural connection force of  $C$  is relatively large, which is consistent with the research results of the basic physical properties discussed above.  $C$  has large water content and a high content of hydrophilic minerals.

### Unloading and reloading characteristic

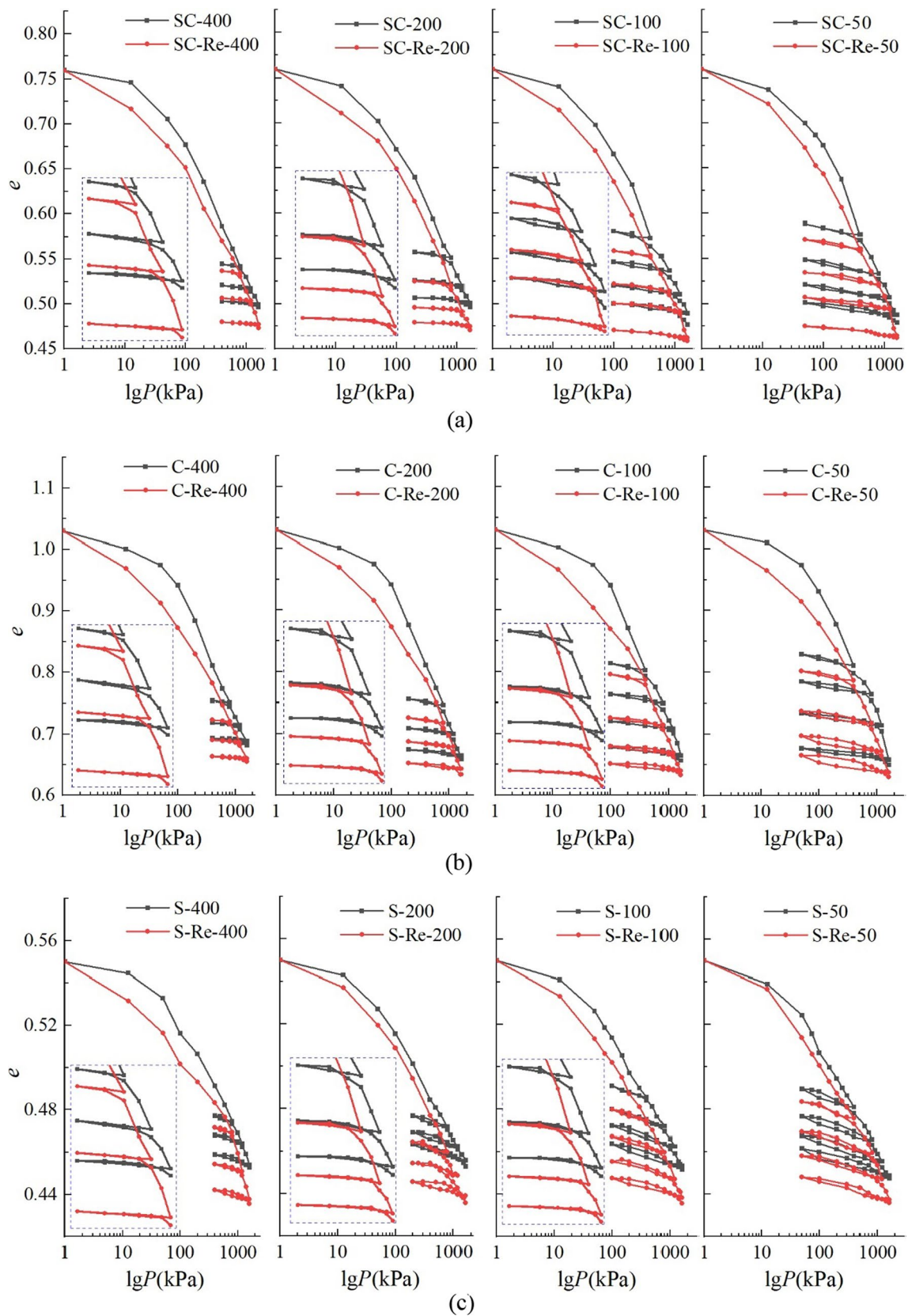
#### Rebound and recompression curve analysis

Figure 6 shows the reciprocating loading and unloading compression test curves of the three soil samples. The  $e$ - $\lg P$  curves of all soil samples obtained in this test have the following characteristics.

- (1) In the test curves, the void ratios of the remodeled samples are all located below the original samples, which is the same as the change of void ratio in the standard consolidation test. During unloading, rebound, and recompression, the void ratio of the remolded samples under the same overburden pressure is lower than that of the original samples.
- (2) Upon unloading curves, a nearly bilinear curve was observed: when the stress was higher than the threshold stresses, the slope was small, and when the stress was lower than the threshold stress, the slope was significantly larger.
- (3) Upon reloading curves, a trilinear curve was identified. Less than the maximum preloading pressure  $P_{max}$  of the cycle, a nearly bilinear curve was again observed, with a small slope at the beginning, and then it goes up. Further loading beyond  $P_{max}$  gave rise to a larger slope, which is most definitely related to the plastic volume changes.

- (4) Under all minimum unloading pressures, the slope of the curve is relatively steep during the initial unloading. It becomes less steep with further unloading for each loading cycle. The slope is relatively steep during initial loading and becomes less steep with an increasing number of loading cycles.
- (5) The reloading curve does not coincide with the rebound curve, forming a hysteresis loop, indicating an irrecoverable plastic deformation in the compression/rebound/recompression deformation of soil. After the compression-rebound, under low and high consolidation pressures, it is found that the hysteresis loop formed by the last stage of the recompression curve and the previous one is significantly greater, indicating that the soil has a greater extent of structural failure and increased plastic deformation. The reason is that the rebound deformation of soil is to restore the elastic deformation of soil in deformation. When the soil mass is in the recompression stage, the load first acts on the previous elastic deformation part of the soil mass. When the soil mass is completely compressed and stabilized, new plastic deformation of the soil mass is generated again, and the hysteresis loop phenomenon occurs after the soil mass undergoes recompression.
- (6) The curve variation characteristics of the three groups of soil samples are similar, but the curve difference between the original sample and the remolded sample is  $C > SC > S$ . This is due to the high content of clay particles, clay minerals, and fine particles in  $C$ , resulting in the high binding water content and strong structure of the original sample.

The additional void ratio defined by Burland (1990) is used to describe the difference between the void ratio of the original soil and the corresponding remolded soil. According



**Fig. 6** Oedometer test with unloading/reloading on different soil samples: **a** SC, **b** C, **c** S



to the compression effect under different stress paths, the change rate of total void ratio and the additional void ratio between the original sample and the remolded sample under different minimum unloading pressure ( $P_{min}$ ) were analyzed, as shown in Fig. 7. With the decrease in  $P_{min}$ , the change rate of the total void ratio of soil samples C and SC exhibited an increasing trend (the original samples increase varied from 33.33 to 37.22%, and 32.5 to 36.9%, respectively, and remolded samples increase varied from 36.87 to 39.22% and 35.2 to 38.8%, respectively). It is particularly emphasized that the change rate of the total void ratio of S under different  $P_{min}$  is relatively stable and less affected by  $P_{min}$ . This is because S is primarily composed of silt and small clay content. The rebound deformation and recompression deformation generated during the addition and unloading are small, and mainly the elastic deformation is observed, which can be recovered. The change rate of the total void ratio of the remolded samples was higher than that of the original samples. With the decrease in  $P_{min}$ , the additional void ratio decreased gradually to 1.89%, 2%, and 2.45%, respectively.

This indicates that cyclic loading and unloading can reduce the compression difference between the original and the remolded samples, but only to a limited extent.

### Rebound and recompression parameter analysis and discussion

The relationship curve between the consolidation pressures and the maximum rebound rate ( $\delta_{max}$ ) of the soil sample under different  $P_{min}$  is shown in Fig. 8. The rebound rate of the original sample is greater than that of the remolded sample, indicating that the amount of rebound of the original sample is greater than that of the remolded sample at the same  $P_{max}$  and  $P_{min}$ . This indicates an error in the design using the rebound amount of the remolded sample in engineering design. It can be seen from the figure that the higher the consolidation pressure, the higher will be the final rebound rate of the rebound deformation after the soil sample is completely unloaded. When  $P_{min}$  is large, the rebound deformation is small or hardly occurs. When  $P_{max}$

**Fig. 7** The void ratio changes rate and the difference between the original sample and the remolded sample: **a** SC, **b** C, **c** S

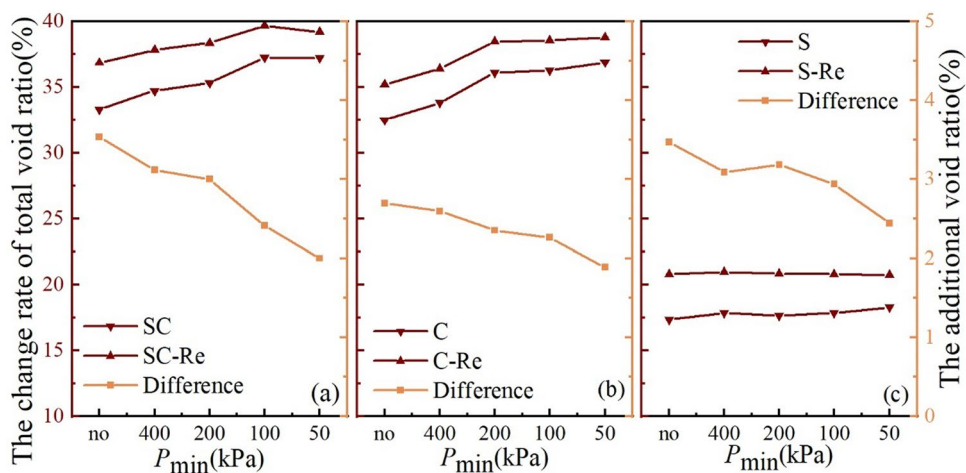
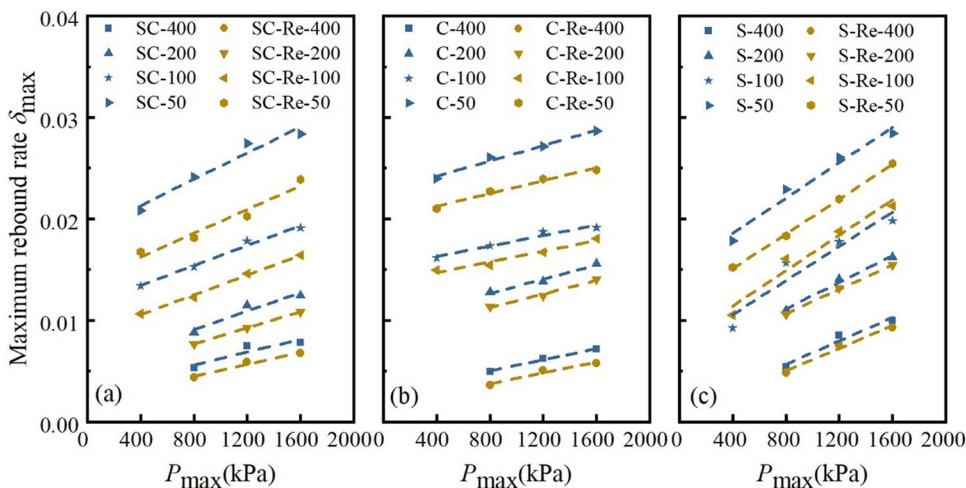


**Fig. 8** The relation curve between the maximum preloading pressure ( $P_{max}$ ) and the maximum rebound rate of the soil sample under different  $P_{min}$ : **a** SC, **b** C, **c** S



is large, the secondary consolidation settlement is even more significant than the rebound deformation, and only when  $P_{\min}$  reaches a certain value can there be obvious rebound deformation. Under the same  $P_{\min}$  and  $P_{\max}$ , the maximum rebound rate  $\delta_{\max}$  of S is much smaller than that of C and SC. According to the relationship curve between  $\delta_{\max}$  and  $P_{\max}$  in Fig. 8, it can be deduced that the larger the  $P_{\max}$ , the greater the soil rebound after unloading. There is an obvious linear relationship between  $\delta_{\max}$  and  $P_{\max}$ ; after the soil rebound deformation is completed,  $\delta_{\max}$  increases linearly with the increase of  $P_{\max}$  (Li et al. 2011). This can also be expressed as the greater the excavation depth of the foundation pit, the greater the rebound of the soil at the bottom of the pit (Zhang et al. 2008). It is worth noting that the change curves of  $\delta_{\max}$  versus  $P_{\max}$  for the remolded and original soil samples show a similar trend. When  $P_{\min}$  is small, the  $P_{\max}$  and  $\delta_{\max}$  fitting lines of the remolded and original soil samples are far apart. With the increase in  $P_{\min}$ , the  $P_{\max}$  and  $\delta_{\max}$  fitting lines of the remodeled and original soil samples are closer due to the difference in the structure of the original soil sample. As  $P_{\min}$  increases to the pre-consolidation pressure  $P_c$ , the difference between the remodeled and original soil samples weakens.

After the soil rebound deformation, the final rebound deformation rate increases linearly with the consolidation pressure, which can be fit for:

$$\delta_{\max} = AP_{\max} + B. \quad (3)$$

According to the mathematical fitting, the final rebound rate of the soil layer can be predicted after the consolidation pressure is determined, and it can be further calculated numerically. It can be seen from the figure that the fitted slope  $A$  changes with  $P_{\min}$ , and the curve of change between  $A$  and  $P_{\min}$  is drawn, as shown in Fig. 9. The value of  $A$  indicates the sensitivity of the maximum rebound rate to the consolidation pressure.

The following pattern can be seen in Fig. 9 for  $A$ .

- (1)  $C < SC < S$ . In other words, the sensitivity of  $\delta_{\max}$  of the C soil sample to consolidation pressure is the lowest, whereas that of the S soil sample is the highest.
- (2) The value of  $A$  for the original sample is larger than that for the remodeled sample.
- (3) With the increase of  $P_{\min}$ ,  $A$  decreases. In particular, the three groups of soil samples showed different changes in  $P_{\min}$  from 100 to 200 kPa: the C soil samples showed an increase, the SC soil samples slowly decreased, and the S soil samples showed a significant decrease.

The deformation of the cohesive soil layer comprises elastic and plastic deformations. Elastic deformation is recoverable after unloading, whereas plastic deformation is

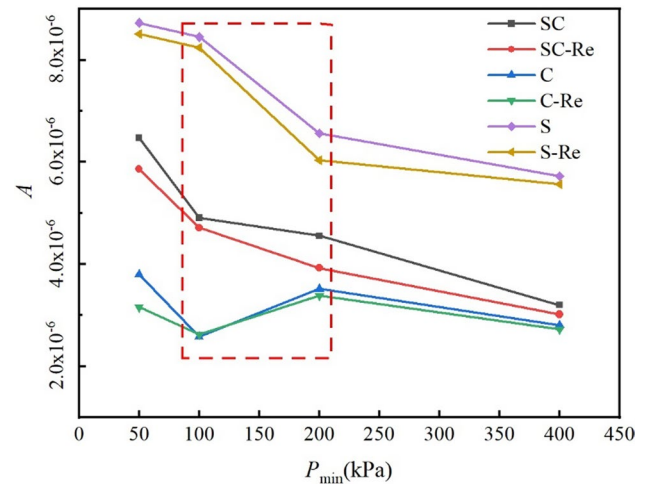


**Fig. 9** Variation curve of  $A$  (the slope of the fitting curve of the maximum rebound rate and the maximum preloading pressure) with  $P_{\min}$

irrecoverable. The larger the proportion of elastic deformation, the more obvious the change in  $\delta_{\max}$  when the consolidation pressure changes. Cohesive soil has mainly plastic deformation. Once compressed and consolidated, most of the deformation cannot be recovered by rebound. On the other hand, sandy soil has primarily elastic deformation (Yang et al. 2018). Therefore, the sensitivity of  $\delta_{\max}$  to consolidation pressure in S is stronger than that of SC. The original soil has produced a certain structure in the natural settlement environment. The recoverable elastic deformation accounts for a high proportion of the force deformation, and the remodeling-like artificial machine is made, and the structure is relatively loose. The proportion of recoverable elastic deformation in the stress deformation is relatively small, so the  $\delta_{\max}$  of the original soil is more sensitive to the consolidation pressure than the remolded soil. The  $\delta_{\max}$ - $P_{\max}$  curve has an evident turning point in the 100–200 kPa section, which is why the  $e$ - $p$  curve has the largest slope at this stage, which is the stage where the soil compressibility is the largest. Since the S in the  $e$ - $p$  curve changes smoothly overall and the slope decreases, a decrease relatively gently, the  $e$ - $p$  curve of C has an obvious turning point at the stage of 100–200 kPa, and the turning point is close to 100 kPa, so the compressibility is the largest at this point. The proportion of elastic deformation in compression deformation is relatively small, so the sensitivity of  $\delta_{\max}$  to consolidation pressure is weak, and the SC property is between C and S.

In the rebound phase, the rebound curve can be expressed in two stages. The turning point of the two stages depends on the mechanical effect (overlying preloading  $P_{\max}$ ) on the one hand and the physicochemical effect on the other hand. According to the curve, the turning point is mainly located at the interval of 100–200 kPa, so a relatively large rebound is generated in this interval. Soil sample C has a

high moisture content, large pore ratio, and high compressibility. Physical and chemical effects are dominant at this stage, and similar rebound characteristics are generated under different preloading. The soil samples of S at this stage were mainly mechanical properties, so they showed a conventional increasing trend with  $P_{min}$  and decreasing trend with S, while SC was in the middle.

The addition curve does not coincide with the rebound curve, forming a hysteresis loop, indicating irreversible plastic deformation in the loading/reloading deformation of soil. Figure 10 shows the curves of recompression rate ( $\lambda$ ) and consolidation pressure under different  $P_{min}$ . It can be seen from Fig. 10 that with the increase of  $P_{max}$ ,  $\lambda$  decreases linearly, showing that with the increase of  $P_{max}$ , the plastic deformation ratio generated by rebound gradually decreases and tends to be elastic. There is a significant difference in  $\lambda$  ( $C > SC > S$ )—the original samples distribution interval was from 2.707 to 1.431, from 1.922 to 1.323, and from 1.424 to 1.11, the remolded sample distribution interval was from 2.567 to 1.47, from 1.942 to 1.361 and from 1.703 to 1.13, respectively.  $\lambda$  of the original sample is lower than that of the remolded sample, which is contrary to the final rebound rate. The excavation of the foundation pit produces rebound, and the construction of buildings and structures produces recompression. The amount of rebound and the amount of recompression need to be determined.

In the recompression deformation stage of the soil,  $\lambda$  decreases with the increase of  $P_{max}$ . The linear fitting equation of  $\delta_{max}$  is used for reference to define the fitting equation of  $\lambda$  as

$$\lambda = A_r P_{max} + B_r \tag{4}$$

The slope,  $A_r$ , of the variation curve of soil samples under different intervals of  $P_{min}$  are shown in Fig. 11. It is observed that the larger is the slope, the more sensitive the recompression rate is to  $P_{min}$ . This shows that any change of the

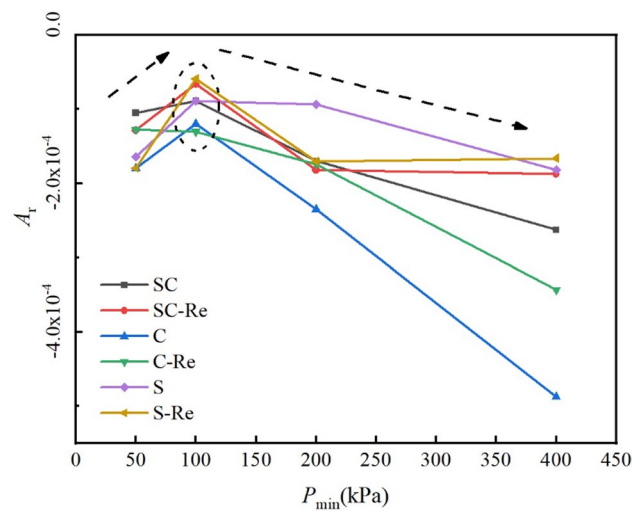
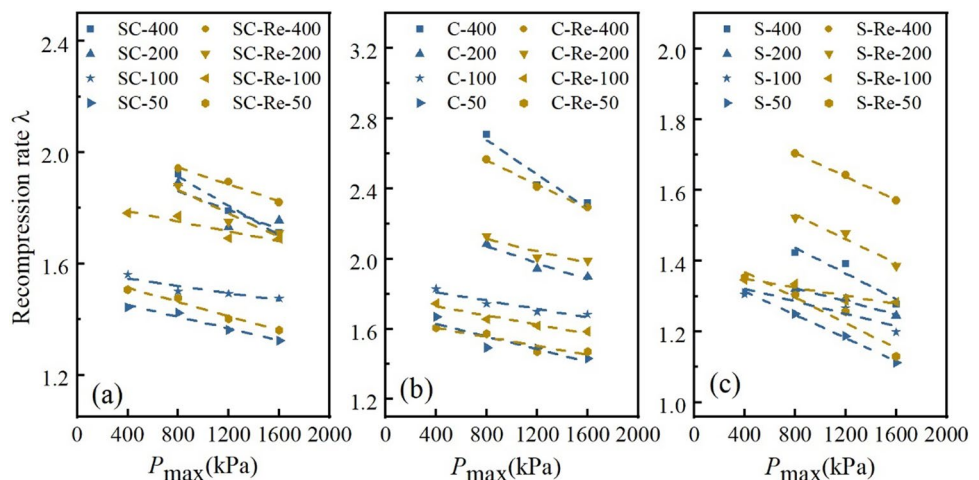


Fig. 11 Variation curve of  $A_r$  (the slope of the fitting curve of the recompression rate and the maximum preloading pressure) with  $P_{min}$

recompression rate results in an expansion trend when  $P_{min}$  changes. It is pertinent to mention that the slope is a negative value, so while discussing the magnitude of the slope  $A_r$ , it refers to the absolute value of  $A_r$ . The following deductions can be made from Fig. 11.

- (1) The  $A_r$  value of the original sample is generally greater than that of the remodeled sample, which signifies the greater sensitivity of the original sample to  $P_{min}$  than the remodeled sample. In other words, When  $P_{max}$  is the same, with the change of  $P_{min}$ , the recompression rate of the original sample changes more obviously. This difference between original soil and remolded soil is particularly prominent in C. The  $A_r$  value of the remodeled sample of S at individual locations is smaller than that of the original sample. This is so because the structure of S is weak; thus, the difference

Fig. 10 The relation curve between the maximum preloading pressure ( $P_{max}$ ) and the recompression rate of the soil sample under different  $P_{min}$ : a SC, b C, c S



between the remolded and original samples is relatively small.

- (2) The overall  $A_r$  value shows a decreasing trend with the increase of  $P_{\min}$ . The general trend is that the decrease of C is the largest, followed by SC, and the change of S is small. It is important to note that at  $P_{\min} = 100$  kPa, Ar has a sudden change point, and this phenomenon occurs in all three soil samples. Comparing the analysis in Fig. 5, the unloading stage of the soil sample is divided into a slowly changing section and a steep changing section. Thus, the intersection points of the two stages are both located near 100 kPa, and the soil samples show a relatively stable state at  $P_{\min} = 100$  kPa. The  $A_r$  changes with  $P_{\max}$  here are relatively small.

### Microscopic pore analyses

It is generally acknowledged that the deformation of soil is elastoplastic. The elastic deformation comes from the elastic contact deformation between the soil particles, the deformation of closed bubbles or compressible elastic fluids. Plastic deformation is mainly caused by the relative movement between particles and the crushing of particles (Li and Guo 2000). In other words, the soil deformation caused by the external force results from the comprehensive influence of factors such as the internal connection structure, particles, and pores. The change of pores and structure is the primary manifestation of the deformation of the structure. The composition of the particles in the soft soil directly affects its deformation characteristics. At the same time, the various interaction forces between the particles and the liquid in the pores will also affect the structure of the soft soil. Therefore, the change in the microstructure will directly affect the macroscopic appearance. Analysis of the microstructure and compression characteristics of structured soft soils can better explain the macroscopic engineering compression characteristics of structured soft soils.

To further analyze the distribution of soil pores, the pore results obtained from mercury intrusion experiments are often divided into different pore regions: micropores ( $< 0.04 \mu\text{m}$ ), small pores ( $0.04\text{--}0.4 \mu\text{m}$ ), mesopores ( $0.4\text{--}4 \mu\text{m}$ ), and macropores ( $> 4 \mu\text{m}$ ) according to literature (Wang and Wang 2000; Wang et al. 2020).

Mercury intrusion test was carried out on the sample after the unloading/reloading test mentioned above. Table 4 shows that the pore size range of the sample is mainly concentrated in small pores and mesopores. During the compression process of different test schemes, the percentage of mesopores has a decreasing trend. As the applied load becomes complicated (the decrease of the  $P_{\min}$ ), the percentage of micropores and small pores showed an increasing trend. The relative content of the corresponding macropores gradually decreases. This shows a large amount of water and

gas discharged under loading and compression, the particles in the soil are gradually contacted, and the soil is compacted.

During compression, the main behavior of coarse particles, such as sand, is the movement of position and the enhancement of inter-occlusion. The compression volume is generally difficult to recover after unloading. When clay with a large void ratio is compressed, only the pores between the aggregates will be compressed. Small pores and the pores in the aggregate remain almost unchanged (Shear et al. 1992). The pores in the aggregate are compressed only when the void ratio is small to a certain extent. Due to the strong cementation of the particles, the pores in the aggregate remain almost unchanged even under remolding. Therefore, the unloading rebound recompression of the soil within the pressure range of this study can be considered as the change and dislocation of pores between aggregates. The particle displacement of the clay layer during the compression process is also accompanied by changes in the thickness of the bound water film. When the consolidation pressure level is low, the pores in the soil are mainly the pores within the aggregates and the pores between particles, and the pores inside the aggregates are the majority. As shown in Fig. 12, with the gradual increase of the consolidation pressure, the soil porosity decreases, and its distribution develops from the pores inside the aggregate to the pores between particles. The film water of the cohesive soil is connected. When the stress increases, the water film between the contact points of soil particles becomes thinner or is squeezed out to become free water, and the soil layer is compressed and deformed due to the closeness of soil particles, resulting in subsidence. After the stress is relieved, the cohesive soil is attracted back by the squeezed bound water due to the wedging effect of the water film, and the water film thickness increases again. The soil layer expands and deforms, resulting in a rebound. When loaded, the structural unit transforms from the edge-surface structure to the surface-base structure and converts back to the edge-surface structure when unloading (Cui et al. 2013). The change process is highly complicated, with many influencing factors, and the experimental sampling is limited. It is difficult to reflect the truest and the most reliable model only with the numerical value of part of the position. With the discharge of water and gas, the content of mesopores is gradually decreasing, and most of the mesopores are converted into tiny pores. On the other hand, the compression process of soil puts the soil in a hardened state. The original sample has more micropores than the remolded sample. This is so because the original sample has a certain arrangement and adjustment of the soil particles and pores due to the stress history of the original sample profile. In contrast, the remolded sample is in the preparation process, and

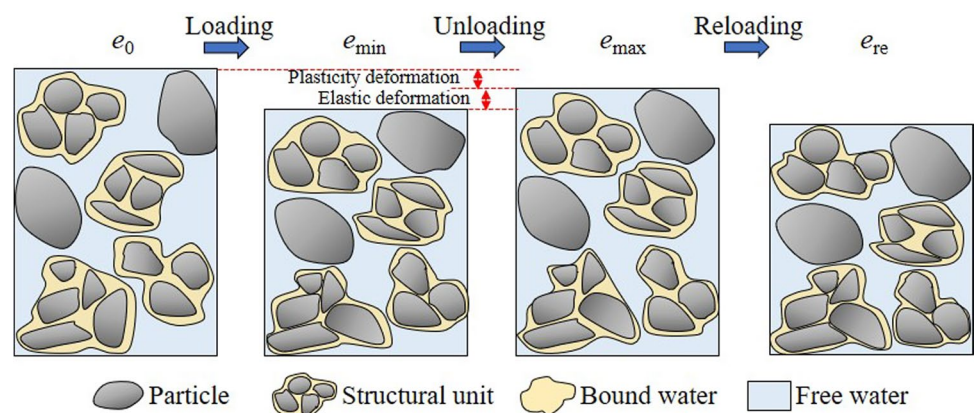


**Table 4** The percentage content of different pore types varies with  $P_{min}$

Sample	Sample type	$P_{min}$ (kPa)	Macropores	Mesopores	Smallpores	Micropores
SC	Original soil	No	13.65	47	31.7	7.65
		400	13.45	47.38	30.35	8.82
		200	9.34	46.18	35.38	9.1
		100	13.26	42.98	34.93	8.83
		50	8.2	38.8	42.3	10.7
	Remolded soil	No	10.13	50.6	34.7	4.57
		400	10.19	43.68	40.34	5.79
		200	10.99	43.87	38.27	6.87
		100	7.87	48.38	38.47	5.28
		50	9.88	42.68	41.97	5.47
C	Original soil	No	12.14	45.86	32.11	10.9
		400	16.09	44.73	30.35	8.82
		200	15.7	41.36	32.87	10.07
		100	14.34	42.91	33.17	9.58
		50	12.81	41.31	36.51	9.37
	Remolded soil	No	18.38	49.48	28.4	3.74
		400	13.83	47.86	33.87	4.44
		200	9.56	45.98	38.07	6.39
		100	10.5	44.67	37.46	7.37
		50	9.12	44.23	36.87	9.78
S	Original soil	No	12.51	53.99	28.38	5.12
		400	9.33	50.82	34.92	4.93
		200	7.96	52.77	33.29	5.98
		100	7.75	49.88	35.98	6.39
		50	11.02	52.04	28.6	8.34
	Remolded soil	No	18.97	52.56	24.16	4.31
		400	18.98	46.94	30.35	3.73
		200	15.02	53.43	25.73	5.82
		100	11.86	46.39	38.06	3.69
		50	9.56	43.87	40.18	6.39

Note:  $P_{min}$ : the minimum unloading pressure

**Fig. 12** Schematic diagram of loading/unloading/reloading microstructure ( $e_0$  is the initial void ratio, and the meanings of  $e_{min}$ ,  $e_{max}$ , and  $e_{re}$  are referred to Fig. 3c)



the force history of the original specimen cannot be completely imitated.

## Conclusion

In this study, the structural soil from Tianjin Binhai New Area was selected as the research object. One-dimensional high-pressure consolidation tests and unloading rebound recompression experiments were carried out. From the microstructure and macroscopic mechanical characteristics, combined with the material composition and mineral composition, three kinds of soil structure were analyzed in the region of the influence of compression rebound and compression characteristic parameter of the rebound.

Following conclusions are drawn from the analysis.

- (1) The compression curve characteristics of remolded and original soils differ significantly. The original soil compression curve presents a piecewise distribution with an obvious inflection point, while the remolded soil compression curve presents a linear change without an obvious inflection point. The compression curve of remolded soil after reduction is used to determine its pre-consolidation pressure. The compression curve of unaltered soil is used to determine the yield stress of the structure. The difference value is the structural strength, and the structural strength of the three soil samples is clay > silty clay > silt.
- (2) In the unloaded rebound recompression curve, the maximum rebound rate and recompression rate of soil are linearly related to the maximum preloaded load. The maximum rebound rate of clay is the least sensitive to the maximum preloaded load, while that of the silt is the largest, and silty clay is in the middle. The sensitivity of clay decreases with the increase of the maximum preloading, and the sensitivity of clay is the least when the minimum unloading pressure is 100 kPa.
- (3) During compression, the pores are readjusted due to the dislocation of particles. The macropores and mesopores are transformed into small pores, finally reaching the state of compression and compaction. There are more micropores in the original soil than in the remolded samples, indicating that the original samples have been compacted to a certain extent during the stress history.

**Funding** This research was funded by International Cooperation and Exchange of the National Natural Science Foundation of China (Grant No. 41820104001); The National Key Research and Development Program of China (Grant No. 2018YFC1505301).

**Data availability** The datasets generated during the current study are available from the corresponding author on reasonable request.

## Declarations

**Conflict of interest** The authors have not disclosed any competing interests.

## References

- Burland JB (1990) On the compressibility and shear strength of natural soils. *Geotechnique* 40(3):329–378. <https://doi.org/10.1680/geot.1990.40.3.329>
- Cui YJ, Nguyen XP, Tang AM, Li XL (2013) An insight into the unloading/reloading loops on the compression curve of natural stiff clays. *Appl Clay Sci* 84(oct.):343–348. <https://doi.org/10.1016/j.clay.2013.08.003>
- Dalla Santa G, Cola S, Secco M, Tateo F, Sassi R, Galgaro A (2019) Multiscale analysis of freeze-thaw effects induced by ground heat exchangers on permeability of silty clays. *Geotechnique* 69:95–105. <https://doi.org/10.1680/jgeot.16.P.313>
- Delage P, Marcial D, Cui YJ, Ruiz X (2006) Ageing effects in a compacted bentonite: a microstructure approach. *Geotechnique* 56(5):291–304. <https://doi.org/10.1680/geot.2006.56.5.291>
- Di Prisco C, Imposimato S, Vardoulakis I (2000) Mechanical modeling of drained creep triaxial tests on loose sand. *Geotechnique* 50(1):73–82. <https://doi.org/10.1680/geot.2000.50.1.73>
- Farzad H, Hamid N (2018) The effect of unloading reloading on the compression behavior of reconstituted clays. *Int J Geomate* 15(51):53–59. <https://doi.org/10.21660/2018.51.52643>
- Jiang MJ, Zhang FG, Hu HJ, Cui YJ, Peng JB (2014) Structural characterization of natural loess and remolded loess under triaxial tests. *Eng Geol* 181:249–260. <https://doi.org/10.1016/j.enggeo.2014.07.021>
- Lambe TW (1967) Stress path method. *J Soil Mech Found Div* 93(6):309–331. <https://doi.org/10.1061/JSFEAQ.0001058>
- Leroueil S, Vaughan PR (1990) The general and congruent effect of structure in natural soils and weak rocks. *Geotechnique* 40(3):467–488. <https://doi.org/10.1680/geot.1990.40.3.467>
- Li ZQ (1982) The mechanics property of underconsolidated soil which have structural strength. *Chin J Geotech Eng* 4(1):34–45
- Li GX, Guo RP (2000) Volume-contraction in unloading of shear tests and reversible dilatation of soils. *Chin J Geotech Eng* 02:158–161. <https://doi.org/10.3321/j.issn:1000-4548.2000.02.003>
- Li JM, Teng YJ (2011) Test study of law of recompression deformation of soil. *Rock Soil Mech* 32(Supp. 2):463–468. <https://doi.org/10.16285/j.rsm.2011.s2.035>
- Li JM, Teng YJ (2018) Regularity and calculation method of rebound deformation and recompression deformation of soil based on bearing test. *Rock Soil Mech* 39(S1):113–121. <https://doi.org/10.16285/j.rsm.2018.0576>
- Li DN, Lou XM, Yang M (2011) Experimental researches on unloading resilient deformation properties during excavations in Shanghai area. *Rock Soil Mech* 32(S2):244–249. <https://doi.org/10.16285/j.rsm.2011.s2.095>
- Lyu HB, Gu JX, Li WJ, Liu FB (2020) Analysis of compressibility and mechanical behavior of red clay considering structural strength. *Arab J Geosci* 13:411. <https://doi.org/10.1007/s12517-020-05352-4>
- Pan LY, Hu ZX (2002) Experimental study on the resilience of pit under unloading. *Chin J Geotech Eng* 24(1):101–104. <https://doi.org/10.16285/j.rsm.2004.08.017>

- Pan LY, Hu ZX, Cheng YM (2001) Experimental study on shear strength of clay under unloading state. *Rock Soil Mech* 22(4):490–493. <https://doi.org/10.16285/j.rsm.2001.04.034>
- Rowe PW (1972) The relevance of soil fabric to site investigation. *Geotechnique* 22(2):195–300. <http://worldcat.org/issn/00168505>
- Shear DL, Olsen HW, Nelson KR (1992) Effects of desiccation on the hydraulic conductivity versus void ratio relationship for a natural clay. *Transp Res Record* 1369:130–135. <http://onlinepubs.trb.org/Onlinepubs/trr/1992/1369/1369-017>
- Shen ZJ (1998) Engineering properties of soft soils and design of soft ground. *Chin J Geotech Eng* 20(1):100–111 (CNKI:SUN:YTGC.0.1998-01-024)
- Shi XC, Wang R, Han Y (2004) Test research on deformation properties of ooze under unloading. *Rock Soil Mech* 08:1259–1262. <https://doi.org/10.16285/j.rsm.2004.08.017>
- Skempton AW (1985) Residual strength of clays in landslides, folded strata, and the laboratory. *Geotechnique* 35(1):1–18. <https://doi.org/10.1680/geot.1985.35.1.3>
- Teng YJ, Gong JF, Li JM (2012) State of arts of foundation engineering technology development. *Chin Civil Eng J* 45(5):126–140. <https://doi.org/10.15951/j.tmgxcb.2012.05.026>
- Teng YJ, Li JM, Wang SG, Gong JF (2013b) Method for recompression deformation of large and deep foundation and its engineering application. *Chin J Geotech Eng* 35(12):2165–2170
- Teng YJ, Li JM, Wang SG (2013a) Experimental study on the method of rebound and recompression deformation calculation in deep and large foundation design. In: *Proceedings of the 18th International Conference on Soil Mechanics and Geotechnical Engineering*. Paris: [s. n.]
- Wang DX, Abriak NE (2015) Compressibility behavior of Dunkirk marine structured and reconstituted soils. *Mar Georesour Geotechnol* 33(5):419–428. <https://doi.org/10.1080/1064119X.2014.950798>
- Wang Q, Wang JP (2000) A Study on fractal of porosity in the soils. *Chin J Geotech Eng* 22:496–498. <https://doi.org/10.3321/j.issn:1000-4548.2000.04.023>
- Wang GX, Xiao SF, Zhou WG (2003) Determination of preconsolidation pressure and structural strength of original structural soils. *Chin J Geotech Eng* 02:249–251. <https://doi.org/10.3321/j.issn:1000-4548.2003.02.030>
- Wang GX, Xiao SF, Huang HW (2005) Determination of stress history of natural structural soft clay. *J Tongji Univ (nat Sci)* 08:1007–1010. <https://doi.org/10.3321/j.issn:0253-374X.2005.08.003>
- Wang DX, Zentar R, Abriak NE (2016) Interpretation of compression behavior of structured and remolded marine soils. *J Mater Civ Eng* 28(6):04016005. [https://doi.org/10.1061/\(ASCE\)MT.1943-5533.0001503](https://doi.org/10.1061/(ASCE)MT.1943-5533.0001503)
- Wang JQ, Wan Q, Kong YY, Han Y, Chen SK (2020) Analysis of the pore structure characteristics of freeze-thawed saline soil with different salinities based on mercury intrusion porosimetry. *Environ Earth Sci* 79:161. <https://doi.org/10.1007/s12665-020-08903-w>
- Xie DY, Qi JL (1999) Soil structure characteristics and new approach in research on its quantitative parameter. *Chin J Geotech Eng* 06:651–656. <https://doi.org/10.1088/0256-307X/16/9/020>
- Yang JL, Yuan HF, Hu YZ, Xu QM, Shi PX, Chen YS (2018) Relationship between elastoplastic deformation of deep clay and land subsidence in Tianjin coastal area. *Rock Soil Mech* 39(10):3763–3772. <https://doi.org/10.16285/j.rsm.2017.1485>
- Zhang SC, Zhang JX, Zhang Y, Ren JD (2008) Experimental study on rebound of clay due to foundation excavation. *Chin J Geotech Eng* 30(S1):426–429 (CNKI:SUN:YTGC.0.2008-S1-092)
- Zhang Y, Xue YQ, Wu JC, Shi XQ, Yu J (2010) Excessive groundwater withdrawal and resultant land subsidence in the Su-Xi-Chang area, China. *Environ Earth Sci* 61(6):1135–1143. <https://doi.org/10.1007/s12665-009-0433-6>
- Zhang Y, Hu Z, Li L, Xue Z (2018) Improving the structure and mechanical properties of loess by acid solutions—an experimental study. *Eng Geol* 244:132–145. <https://doi.org/10.1016/j.enggeo.2018.07.023>
- Zhang XD, Lu YT, Yao J, Wu YJ, Tran QC, Vu QV (2020) Insight into conditioning landfill sludge with ferric chloride and a Fenton reagent: effects on the consolidation properties and advanced dewatering. *Chemosphere* 252:126528. <https://doi.org/10.1016/j.chemosphere.2020.126528>

**Publisher's Note** Springer Nature remains neutral with regard to jurisdictional claims in published maps and institutional affiliations.

Springer Nature or its licensor (e.g. a society or other partner) holds exclusive rights to this article under a publishing agreement with the author(s) or other rightsholder(s); author self-archiving of the accepted manuscript version of this article is solely governed by the terms of such publishing agreement and applicable law.